Clays and Clay Minerals, Vol. 51, No. 5, 543–554, 2003.

ANOMALOUS REVERSE ZONING OF SAPONITE AND CORRENSITE CAUSED BY CONTACT METAMORPHISM AND HYDROTHERMAL ALTERATION OF MARLY ROCKS ASSOCIATED WITH SUBVOLCANIC BODIES

Isabel Abad[1], Juan Jiménez-Millán[1,*], José Miguel Molina[1], Fernando Nieto[2] and Juan Antonio Vera[3]

[1] Departamento de Geología, Universidad de Jaén, Campus Universitario, 23071 Jaén, Spain
[2] Departamento de Mineralogía y Petrología and IACT, Facultad de Ciencias, Universidad de Granada-CSIC, 18002 Granada, Spain
[3] Departamento de Estratigrafía y Paleontología, Universidad de Granada, Facultad de Ciencias, 18071 Granada, Spain

Abstract—The effects of a subvolcanic intrusion on its host rocks in the Priego de Córdoba area (SE Spain) was studied by optical microscopy, X-ray diffraction and electron microscopy. The intrusion of a laccolith of stratiform dolerite in partially consolidated marly sediments at quite shallow depths below the ocean floor took place during the intracontinental rifting phase of the Subbetic zone of the Betic Cordilleras. In the first stage, contact metamorphism caused the crystallization of calc-silicate consisting of grossular andradite garnet, diopside, vesuvianite and titanite for which the upper temperature limit was 500ºC. Phyllosilicates are found in a network of veins cross-cutting the carbonate and calc-silicate matrix, indicating their formation during a process of hydrothermal alteration superimposed on the contact aureole. In the area closest to the subvolcanic rocks, saponite is the main phyllosilicate although some dispersed chlorite is found. In the zone furthest from the contact, corrensite together with saponite and beidellitic smectites were observed. The presence of low-temperature phases (saponite) in the area closest to the laccolith reveals the evolution of the hydrothermal system toward cooler conditions. In the early stage, the circulation of a hot hydrothermal fluid caused the crystallization of chlorite in the area surrounding the subvolcanic body and corrensite in the more distal area, which might have begun even during the contact metamorphism stage. A cooling phase followed, resulting in the crystallization of saponite in the host rocks, and the crystallization of dioctahedral and trioctahedral smectites inside the subvolcanic body.

Key Words—Beidellite, Betic Cordilleras, Contact Metamorphism, Corrensite, Electron Microscopy, Hydrothermal Alteration, Laccolith, Saponite, Subvolcanic Intrusion, X-ray Powder Diffraction.

INTRODUCTION

Intrusions of small subvolcanic bodies in submarine rocks can provide the required heat for developing thermal effects in the host rocks (Vitali *et al.*, 1999) and hydrothermal systems generated by fluid circulation (Fulignati *et al.*, 1997; Dudoignon *et al.*, 1997). The processes of rock-fluid interaction commonly produce phyllosilicates. The formation of clay minerals by the alteration of volcanic rocks in oceanic crust has been studied extensively in the last few years (Bettison-Varga and Mackinnon, 1997; Dudoignon *et al.*, 1997; Pichler *et al.*, 1999) due to its important role in controlling the global distribution of elements and the evolution of the physical properties of the oceanic basement (Honnorez, 1981; Laverne, 1987; Adamson and Richards, 1990). Clay mineral assemblages have been used as indicators of the prevailing conditions of diagenetic and hydrothermal processes that affect marine sediments hosting volcanic bodies (Vitali *et al.*, 1999). Ferromagnesian smectites, corrensite and chlorite are widespread products of hydrothermally-altered mafic rocks. Most of these studies have dealt predominantly with metapelitic rocks (Merriman *et al.*, 1986; Roberts *et al.*, 1990; Bühmann, 1992), whereas phyllosilicates in marly rocks intruded by basaltic rocks have been less extensively studied. A representative case is that of the Guyamas studies at ODP Site 477 by Kelts (1982) and Einsele (1986).

This work aims to constrain the control that a near-ocean-floor subvolcanic intrusion, the Priego de Córdoba laccolith (Figure 1a,b), produced on the sedimentation, and to characterize the metamorphic and hydrothermal effects of the intrusion on its host marls and marly limestones. The study of phyllosilicates generated during the processes of fluid-sediment interaction produced by the emplacement was of particular interest. Samples were studied using a variety of techniques, including powder X-ray diffraction (XRD), scanning electron microscopy (SEM) and transmission and analytical electron microscopy (TEM-AEM) to determine the textural and compositional features of the sedimentary, metamorphic and hydrothermal associations, defining the stages of interaction among host rock, intrusive rock and fluids.

GEOLOGICAL SETTING

The Betic Cordilleras (Southern Spain) comprise the westernmost European Alpine chain (Figure 1a). The

* E-mail address of corresponding author:
jmillan@ujaen.es
DOI: 10.1346/CCMN.2003.0510508

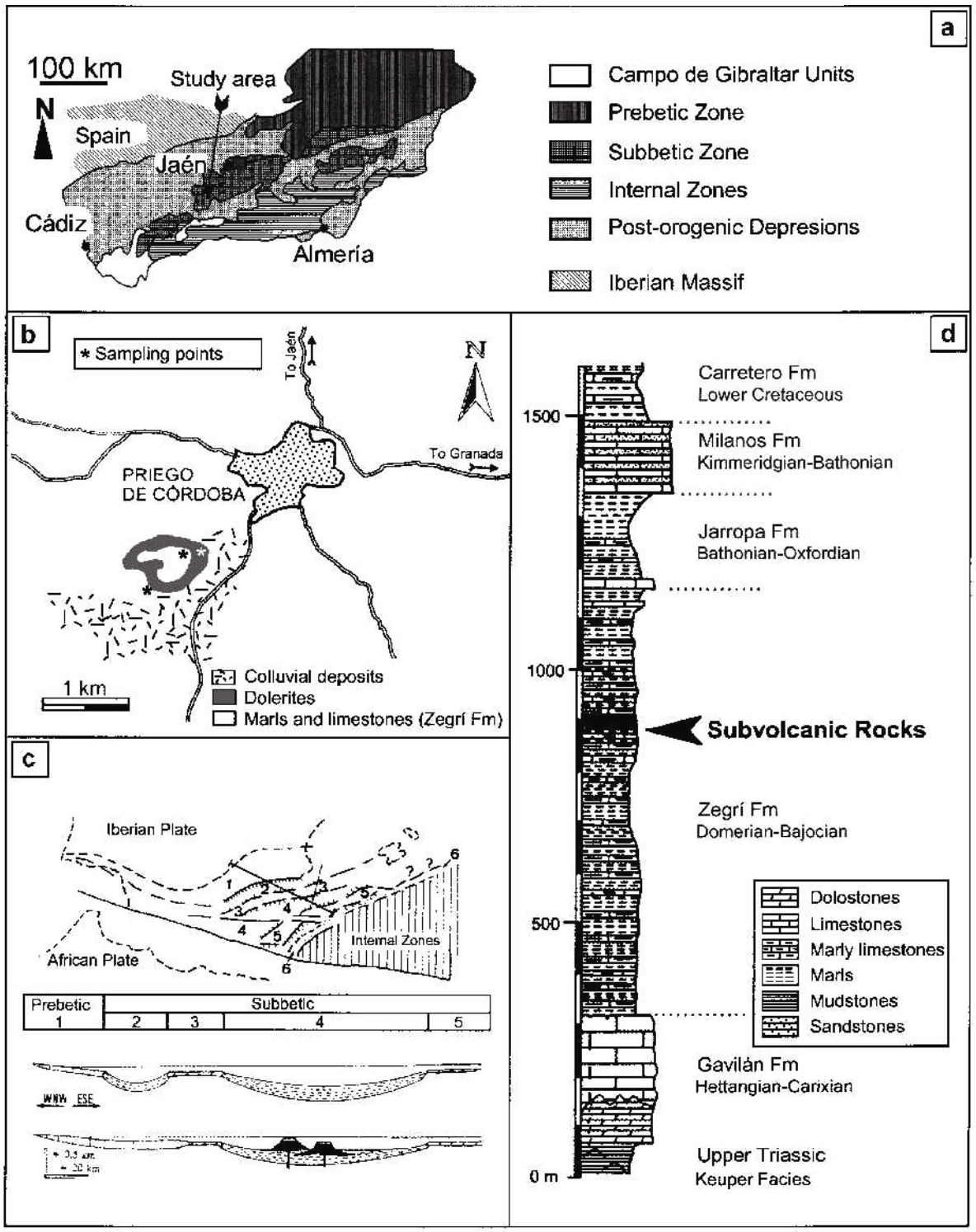

Figure 1. (a) and (b) Geographic and geological context of the study area. (c) Paleogeographic reconstruction of the Western Mediterranean area during the Middle Jurassic including the palinspastic reconstruction cross-sections of the southern Iberian continental margin during the Middle Toarcian (upper cross-section) and the Upper Bajocian-Bathonian (lower cross-section). (1) Prebetic; (2) Intermediate Domain; (3) External Subbetic; (4) Median Subbetic; (5) Internal Subbetic; (6) minimum thickness area of continental crust (after Vera *et al.*, 1997, modified). (d) Stratigraphic column of the Sierra de Priego de Córdoba showing the position of subvolcanic rocks (after Molina and Vera, 2001).

https://doi.org/10.1346/CCMN.2003.0510508 Published online by Cambridge University Press

External Zones (Prebetic and Subbetic) of the Cordilleras are composed mainly of sedimentary rocks deposited from the Triassic to the early Miocene in the South Iberian continental margin. The Subbetic Zone corresponds to the part of the margin in which early Jurassic pelagic facies dominated. Four paleogeographic domains in the middle and late Jurassic can be differentiated in this zone. Jurassic igneous activity appears only in the Median Subbetic (Figure 1c) (Portugal *et al.*, 1995; Vera *et al.*, 1997; Molina and Vera, 1999). The composition of the igneous rocks is mafic with transitional-alkaline affinity (Portugal *et al.*, 1995). Radiometric dating shows maximum igneous activity from 170 to 155 Ma (Figure 1c) (Portugal *et al.*, 1995; Vera *et al.*, 1997) coinciding with the main phase of intracontinental rifting of the South Iberian continental margin. Although basalts with pillow-lava flows dominate, some subvolcanic intrusive dikes, sills and laccoliths can be found. The host rock generally corresponds to the Zegrí Formation (Figure 1d) which consists of Domerian to Bathonian limestone and marl rhythmites. The volcanic edifices are overlain by oolitic limestones deposited on isolated shallow-marine carbonate platforms interpreted as guyots (Vera *et al.*, 1997; Molina and Vera, 1999). The Zegrí Formation also contains local intrusive laccoliths of stratiform dolerites that crop out in small areas (of a few km). They are 60–100 m thick and produced contact metamorphism in the host rocks. One of the best examples lies in the Sierra de Priego de Córdoba where the intrusion has an outcrop extent of 1 km and a maximum thickness of 60 m (Figure 1b). The stratiform dolerites are intruded between Toarcian and Aalenian rocks of the Zegrí Formation. The intrusion may, therefore, have been contemporaneous with the most active phases of the Subbetic volcanism (Aalenian-Bajocian) and thus would have been no more than 4–10 Ma younger than the host rock. Limestones and marls of the Zegrí Formation show mudstone and wackestone microfacies. Toarcian rocks that overly the subvolcanic body develop synsedimentary erosive surfaces that have been interpreted as scar slumps. Figure 2 shows the sampling points and the contact between the sedimentary and igneous rocks.

ANALYTICAL METHODS

Samples were studied using optical microscopy, XRD, SEM with EDX microanalyzer, electron microprobe analyzer (EMPA), HRTEM and AEM.

X-ray diffraction data were obtained from powders and oriented aggregates with two different diffractometers: (1) a Siemens D-5000 diffractometer using CoKα radiation and Fe filter (Universidad de Jaén); and (2) a Philips 1710 powder diffractometer with CuKα radiation, graphite monochromator and automatic divergence slit (Universidad de Granada). Ethylene glycol and heat treatments were performed to corroborate the identification of smectite and corrensite on the basis of the expandibility of these phases (Figure 3).

The SEM study was made on polished samples with two different microscopes: (1) A Zeiss DSM-950 electron microscope equipped with a Link QX2000 microanalyzer (Universidad de Granada). The following compounds were used as calibration standards: albite, orthoclase, periclase, wollastonite and synthetic oxides (Al_2O_3, Fe_2O_3 and $MnTiO_3$). Analytical data were ZAF corrected. (2) A Jeol 5800 electron microscope equipped with a Link Isis microanalyzer at 20 kV (Universidad de Jaén). In both cases, observations were made using backscattered electron images in the atomic number contrast mode.

Some mineral compositions were determined using a Jeol 8600 Superprobe automated electron microprobe with four wavelength-dispersive spectrometers and one energy-dispersive spectrometer Tracor Northern (Noran) TN 5500 (Johns Hopkins University). The EMPA was operated under the following conditions: accelerating voltage 15 kV, probe current 20 nA, electron beam diameter <5 μm. The following compounds were used as calibration standards: albite, orthoclase, anorthite, enstatite, rhodonite, anatase and fayalite. Data correction was performed with program CITZAF (Armstrong, 1989).

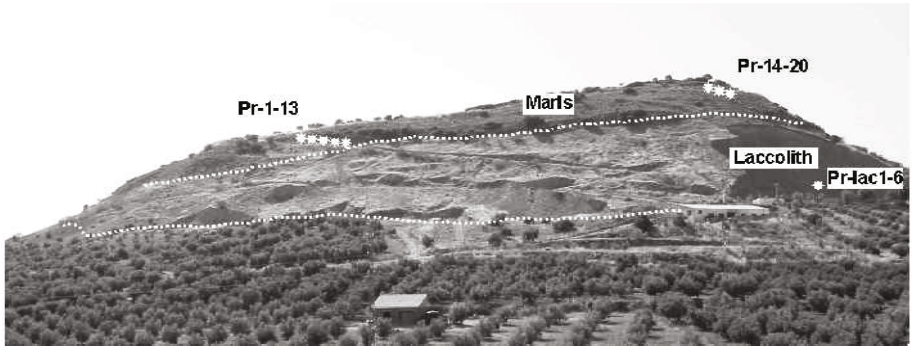

Figure 2. Panoramic view of the outcrop from the south of the laccolith. The sampling points (*) and the contact between the subvolcanic rocks and the host rocks (dashed line) are indicated.

https://doi.org/10.1346/CCMN.2003.0510508 Published online by Cambridge University Press

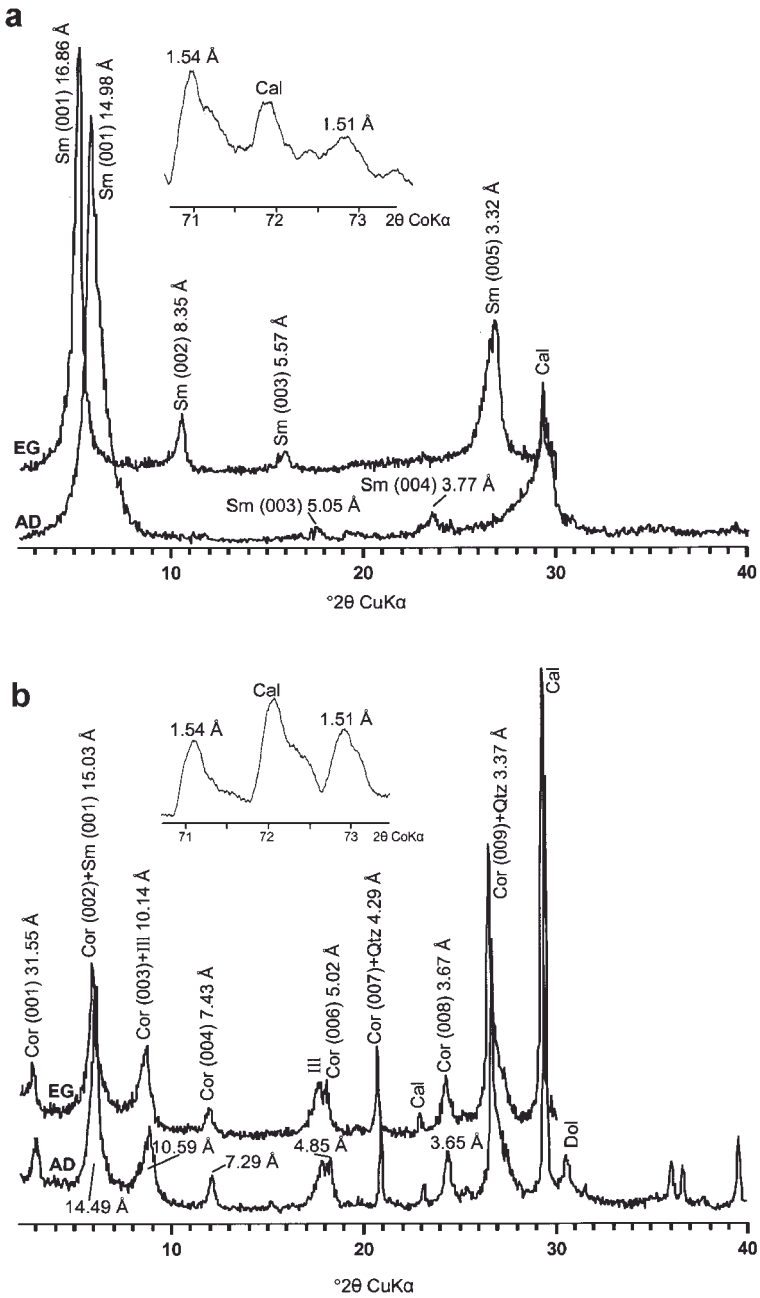

Figure 3. XRD patterns of air-dried (AD) and ethylene glycol (EG) solvated materials: (a) sample from zone 1; (b) sample from zone 2. The 001 reflection of glycolated smectite is superposed on the 002 reflection of corrensite.

The HRTEM studies were performed with a Philips CM-20 scanning transmission electron microscope (STEM) working at 200 kV. The point to point resolution is 2.7 Å in the TEM mode and 50 Å in the STEM mode. Copper rings were attached to representative selected areas of the thin-sections. These areas were detached through gentle heating. Samples were further thinned with a Gatan dual ion mill using an acceleration voltage of 6 kV during three stages: (1) incidence angle of 15° and probe current of 1 nA; (2) incidence angle of 15° and probe current of 0.6 nA; (3) incidence angle of 12° and probe current of 0.4 nA. Chemical analyses of particles were made in the STEM mode with an EDAX micro-analysis system. A 200 × 1000 Å scanning area with the long axis oriented parallel to phyllosilicate packets was used for each analysis using a 50 Å beam diameter. Counting times of 200 s were used except for Na and K, which were analyzed using 30 s counting times. Albite, olivine, biotite, spessartine, muscovite, chlorite and titanite were used to obtain k factors for transformation

https://doi.org/10.1346/CCMN.2003.0510508 Published online by Cambridge University Press

Table 1. Structural formulae for smectites of the laccolith normalized to $O_{10}(OH)_2$.

Analysis	Si	^{IV}Al	^{VI}Al	Mg	Fe	Σoct	Na	K	Ca	Na+K+Ca
Pr-1ac6	3.11	0.89	0.44	0.73	1.12	2.29	0.00	0.06	0.33	0.39
Pr-1ac5	3.41	0.59	0.24	1.10	1.08	2.42	0.00	0.03	0.19	0.21
Pr-1ac4	3.31	0.69	0.18	1.78	0.71	2.67	0.00	0.03	0.22	0.25
Pr-1ac3	3.31	0.69	0.42	1.14	0.92	2.48	0.00	0.00	0.20	0.20
Pr-1ac2	3.23	0.77	0.76	0.92	0.76	2.45	0.00	0.00	0.18	0.18
Pr-1ac1	3.32	0.68	1.68	0.17	0.19	2.05	0.21	0.00	0.25	0.46

AEM analyses. Total Fe considered as Fe^{2+}

of intensity ratios to concentration ratios according to the Cliff and Lorimer (1975) approximation.

MINERALOGICAL AND PETROLOGICAL CHARACTERIZATION

Igneous intrusion

The mineralogical and petrographic features of the Priego de Córdoba subvolcanic intrusive laccolith and its contact metamorphism were studied by Busnardo and Chenevoy (1962). This laccolith consists of stratiform dolerites with poikilitic texture containing 90% of zoned calcic plagioclase (An_{85} at the core to An_{16} at the border), and 10% of augitic pyroxene with Ti. Ilmenite, biotite and apatite are accessory minerals. Most of the exposed rocks are poorly compacted due to clay minerals replacing plagioclase and augite. The XRD patterns show a smectite phase with a basal spacing of 15.8 Å that expands to 16.9 Å after ethylene glycol treatment. Furthermore, the presence of two distinct 060 peaks at 1.49 and 1.53 Å reveal that both dioctahedral and trioctahedral smectites are present. Some TEM-AEM microanalyses (Table 1) have an Al-rich dioctahedral beidellite-like composition (analysis Pr-lac1). In contrast, the composition of analysis Pr-lac4 is closer to ferromagnesian saponite. However, most smectites from the laccolith plot between the theoretical positions of saponite and beidellite (Figure 4). Saponite-beidellite mixtures have been reported as products of submarine alteration of mafic rocks using EMPA and SEM analyses (Pichler *et al.*, 1999; Clayton and Pearce, 2000). Hydrothermal synthesis experiments by Decarreau *et al.* (1992) and Yamada *et al.* (1999) suggested the immiscibility of these two smectites below 400ºC. Therefore, as smectites from the laccolith were studied by AEM, our data probably represent analyses of intimately mixed species even at a TEM scale. Beidellite-saponite mixtures were synthesized experimentally by Grauby *et al.* (1993). Their AEM data showed that the Al-Mg series was continuous between these two end-members. Their XRD and infrared data have, however, shown that the clay particles were made up of clusters of two different structures and solid-solution presents a wide miscibility gap. Huertas *et al.* (2000) obtained AEM analyses of synthesized particles with intermediate composition which were interpreted as being due to topotactic growth of dioctahedral smectite on trioctahedral smectite lamellae.

Host rocks

The host marly rocks developed several mineralogical and textural changes produced by the subvolcanic body. Two mineral zones from the contact with the subvolcanic body to the unaffected sediments were identified depending on the distance from the intrusion.

Zone 1. The host rocks closest to the laccolith (~10 m) appear strongly brecciated. These rocks have a calcite-

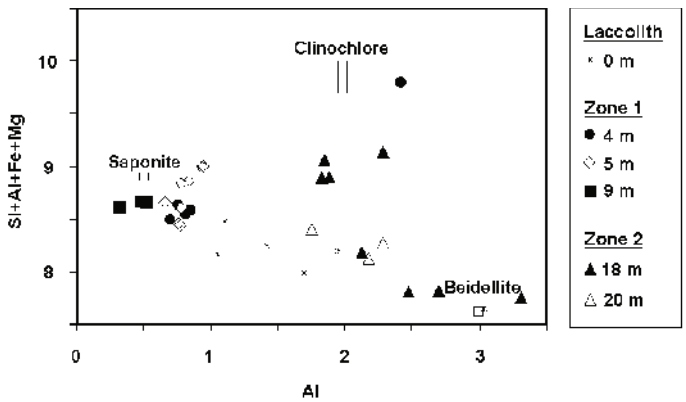

Figure 4. Compositional diagram of total Al *vs.* Si+Al+Fe+Mg. Phyllosilicate analyses normalized to 28 charges. The theoretical projection of each mineral phase is indicated by an open square. Based on a diagram proposed by Schiffman and Fridleifsson (1991).

https://doi.org/10.1346/CCMN.2003.0510508 Published online by Cambridge University Press

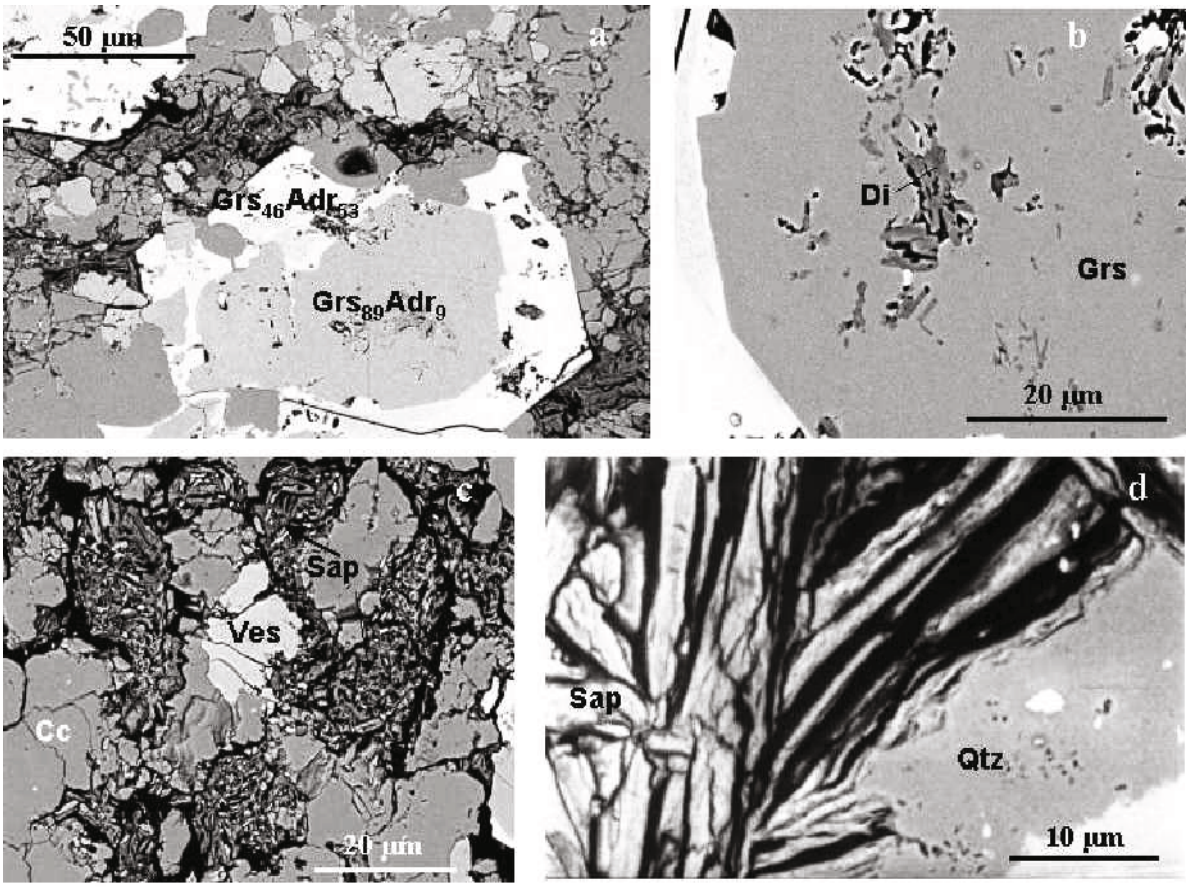

Figure 5. BSE images: (a) partial textural aspect of the host rocks closest to the laccolith showing garnets of the Ca-silicate association (see text for explanation); (b) detail of garnet with small diopside inclusions; (c) small poorly crystalline saponites filling the vein network; (d) larger subidiomorphic saponites intensely fractured. Adr: andradite; Cc: calcite; Di: diopside; Grs: grossular; Qtz: quartz; Sap: saponite; Ves: vesuvianite.

rich matrix with mosaic texture containing dispersed Ca-rich silicate crystals 10–50 µm in size. The carbonate matrix is crosscut by a network of greenish-brown phyllosilicate veins.

Ca-rich silicates. The Ca-silicate association consists of garnet, diopside, vesuvianite and titanite. The back-scattered electron (BSE) images reveal the presence of two generations of garnets (Figure 5a). Both types have high Ca contents, ~3 atoms per formula unit (a.p.f.u.) normalized to 12 oxygens (Table 2). Diopside appears as small inclusions in the garnet (Figure 5b) or as dispersed crystals in the carbonate matrix. These minerals frequently show textural evidence of instability, such as irregular borders in the phyllosilicate-filled veins (Figure 5c).

Clay minerals. The network of veins cross-cutting the host carbonate matrix is filled by clay minerals. Studies by XRD, EMPA, SEM-EDX and HRTEM-AEM allowed the identification of saponite and chlorite. Saponite occurs as the dominant phyllosilicate. The XRD patterns show a d_{001} of 14.98 Å expanding to 16.86 Å after ethylene glycol treatment (Figure 3a). Chemical and

Table 2. Structural formulae for garnets normalized to 12 oxygens.

Analysis	Si	Ti	Al	Fe	Mn	Mg	Ca	Andradite	Pyrope	Spessartine	Grossular
I.1	2.99	0.01	1.81	0.16	0.01	0.07	2.95	8.35	2.30	0.25	89.09
I.2	2.98	0.00	1.81	0.19	0.01	0.04	2.96	9.75	1.37	0.36	88.52
II.1	2.98	0.01	0.92	1.06	0.01	0.01	3.02	53.57	0.20	0.47	45.76
II.2	3.00	0.01	0.88	1.08	0.02	0.01	3.00	55.11	0.40	0.66	43.83
II.3	3.01	0.01	1.05	0.93	0.01	0.01	2.99	46.97	0.28	0.40	52.35

EMPA analyses. Total Fe considered as Fe^{3+}

https://doi.org/10.1346/CCMN.2003.0510508 Published online by Cambridge University Press

textural features distinguish two types of saponite. Poorly crystallized grains, 5–10 μm in size, located in the network of veins in the matrix (Figure 5c) are abundant. The Mg content of this saponite ranges from 1.46 to 2.19 a.p.f.u. normalized to 22 charges (Table 3a). The main cation in the interlayer is Ca, ranging from 0.12 to 0.40 a.p.f.u. The K and Na contents are always <0.05 a.p.f.u. Intensely fractured subidiomorphic crystals of larger saponites (up to 100 μm) (Figure 5d) are richer in Mg (up to 2.36 a.p.f.u.) and poorer in Ca (~0.08 a.p.f.u.). In addition, Na is the most important interlayer cation (up to 0.19 a.p.f.u.). Both types of saponite have an important substitution of Si for Al in the tetrahedral position. Figure 4 shows a slight scattering of the smectite composition unrelated to the sampling point positions. Some saponites in Zone 1 possess rather low totals (average 7.07 a.p.f.u.) as compared with an ideal composition. However, this compositional feature has been reported previously for saponites formed in hydrothermal systems (*i.e.* Dudoignon *et al.*, 1997, with average total of 6.73 a.p.f.u.; Hunter *et al.*, 1999, with average total of 7.10 a.p.f.u.), and could be related to the presence of a small number of layers or clusters of dioctahedral smectites.

At the lattice scale, the saponite shows the typical texture of smectite, with unoriented packets that coalesce or open (see low-magnification image in Figure 6). The packets are ~100–200 Å thick and never more than 400 Å, with wavy orientations and layer terminations. The electron beam generates fissures parallel to the layers and produces their collapse by dehydration under high-vacuum conditions, thus explaining the 10 Å periodicity of the lattice fringes (Figure 7). However, this texture is very different from that characterizing detrital smectites (*e.g.* Figure 4 in Nieto *et al.*, 1996) which are formed by anastomosing layers, with continuous changes in spacing and orientation, and no recognizable layered packets. This type of texture was described as megacrysts by Peacor (1992). Despite their different chemical composition, the Priego saponites have a texture intermediate between that of the detrital dioctahedral smectites and the retrograde-diagenetic dioctahedral smectites. Small and defect-free packets of smectites formed by the chlorite alteration due to fluid circulation were described by Nieto *et al.* (1994, Figure 7) in the Maláguide Complex.

The BSE images and EMPA analyses allowed the identification of chlorite at 4 m from the contact. Its chemical composition (average: $(Si_{2.88}Al_{1.12})(Al_{1.29}Fe_{1.59}Mg_{2.97})_{\Sigma oct.=5.85}$) reveals that this trioctahedral chlorite is a clinochlore with a Fe/(Fe+Mg) ratio of 0.35. The octahedral vacancy of 0.15 a.p.f.u. (normalized to 28 charges) represents a common characteristic of chlorites of hydrothermal origin (Shau and Peacor, 1992).

Zone 2. In this interval the marly limestone and marl rhythmite do not have the contact metamorphism mineral paragenesis described in Zone 1. Optical and SEM-EDX studies reveal that these rocks consist of a calcitic matrix containing clay minerals, quartz, rutile and dispersed detrital white mica. Some rocks have developed a low-density vein network filled with calcite and clay minerals. The XRD data and TEM-AEM reveal the presence of smectite and corrensite.

Smectite was detected in the XRD diagrams from its 14.49 Å spacing. The XRD patterns indicate the coexistence of dioctahedral and trioctahedral smectites characterized by two 060 peaks at 1.51 Å and 1.54 Å (Figure 3b). In HRTEM images, smectite zones occur as wavy 10 Å fringes with fissures parallel to the layers caused by the incident electron beam. The AEM analyses of smectites from this zone (Table 3b) reveal a wide compositional interval for Al (2.60 to 1.38 a.p.f.u.) and Mg (0.18 to 1.43 a.p.f.u.). Analyses poorer in Mg are

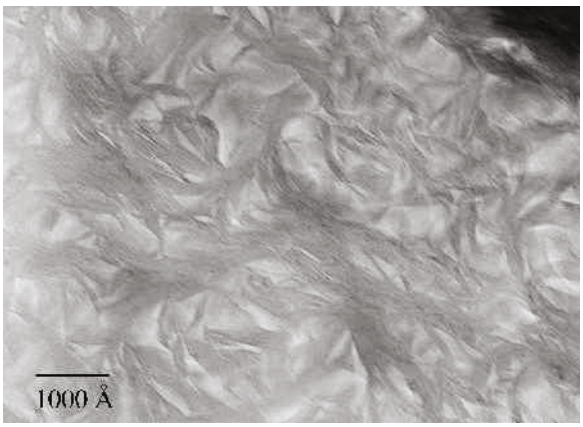

Figure 6. Low-magnification TEM image showing the characteristic textural appearance of the smectitic phases at nanometer scale (sample Pr-2b, Zone 1).

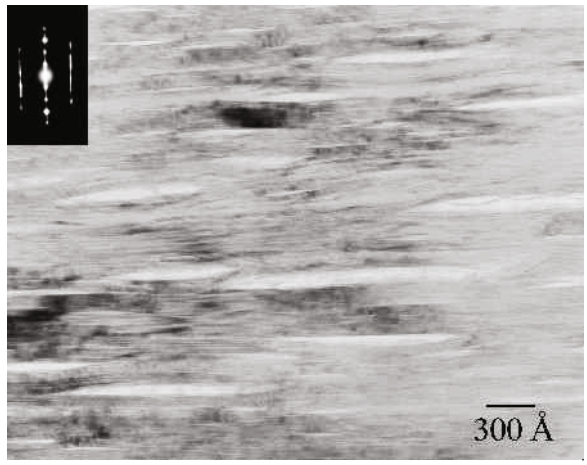

Figure 7. Lattice-fringe image of smectites with slightly curved 10 Å layers and fissures caused by the high-vacuum conditions (sample Pr-2b, Zone 1).

https://doi.org/10.1346/CCMN.2003.0510508 Published online by Cambridge University Press

Table 3. (a) Structural formulae for smectites of Zone 1 normalized to $O_{10}(OH)_2$.

	Distance (m)	Si	^{IV}Al	^{VI}Al	Mg	Fe	Σoct	Na	K	Ca	Na+K+Ca
Saponite I											
Pr-4a-24[a]	4	3.75	0.25	0.30	1.74	0.63	2.67	0.05	0.02	0.27	0.33
Pr-4a-25[a]	4	3.70	0.30	0.29	1.97	0.53	2.79	0.05	0.01	0.19	0.24
Pr-4a-2[b]	4	3.42	0.58	0.06	2.06	0.60	2.72	0.00	0.02	0.24	0.25
Pr-4a-1[b]	4	3.31	0.67	0.00	2.19	0.57	2.77	0.00	0.04	0.31	0.35
Pr-2b-4[b]	5	3.47	0.53	0.08	1.88	0.99	2.95	0.05	0.03	0.18	0.25
Pr-2b-3[b]	5	3.72	0.28	0.34	1.61	0.80	2.75	0.02	0.00	0.13	0.15
Pr-2b-9′[b]	5	3.22	0.60	0.00	1.78	1.05	2.83	0.00	0.00	0.31	0.31
Pr-2b-3′[b]	5	3.54	0.46	0.05	1.46	1.29	2.80	0.00	0.00	0.40	0.40
Pr-2b-2′[b]	5	3.26	0.61	0.00	1.77	1.00	2.77	0.00	0.00	0.30	0.30
Pr-13-38[a]	9	3.96	0.04	0.21	1.90	0.66	2.77	0.01	0.01	0.12	0.15
Pr-13-117[a]	9	3.79	0.21	0.16	2.05	0.61	2.82	0.01	0.01	0.19	0.21
Pr-13-119[a]	9	3.73	0.27	0.14	2.01	0.65	2.81	0.01	0.00	0.23	0.25
Saponite II											
Pr-2b-14[c]	5	3.40	0.60	0.13	2.30	0.65	3.07	0.19	0.00	0.07	0.26
Pr-2b-17[c]	5	3.39	0.61	0.13	2.36	0.59	3.08	0.17	0.00	0.08	0.24

[a] EMPA analyses. [b] AEM analyses. [c] EDX analyses. Total Fe is assumed to be Fe^{2+}

(b) Structural formulae for smectites of Zone 2 normalized to $O_{10}(OH)_2$.

	Distance (m)	Si	^{IV}Al	^{VI}Al	Mg	Fe	Σoct	Na	K	Ca	Na+K+Ca
Smectite											
Pr-15-3[a]	20	3.18	0.82	0.97	1.08	0.44	2.49	0.00	0.17	0.11	0.27
Pr-15-2[a]	20	3.35	0.65	0.73	1.43	0.43	2.59	0.00	0.06	0.12	0.17
Pr-15-1[a]	20	3.22	0.78	0.93	1.09	0.36	2.38	0.00	0.17	0.24	0.41
Pr-18-3[b]	18	3.22	0.78	1.82	0.18	0.09	2.09	0.00	0.23	0.23	0.46
Pr-18-3[b]	18	3.57	0.43	1.69	0.37	0.09	2.14	0.00	0.22	0.12	0.34
Pr-18-1[b]	18	3.58	0.42	1.52	0.49	0.12	2.14	0.00	0.30	0.13	0.44

AEM analyses. Total Fe assumed to be Fe^{2+}
[a] Vein materials
[b] Sediment matrix

found in the dispersed sediments while those richer in Mg are located in the veins. Even in the Al-richer analyses, some cation totals are excessively high for dioctahedral smectite. With the exception of higher K (up to 0.3 a.p.f.u.), these analyses do not differ substantially from some of those obtained in the laccolith smectites. Therefore, these analyses could also be mixtures of dioctahedral and trioctahedral smectite and both types of smectites are present in the dispersed sediments as well as the veins. Ortega-Huertas *et al.* (1991) observed that beidellitic smectite is one of the most characteristic minerals in those Zegrí Formation sediments which have not been affected by volcanic intrusions. The Al-smectite shows the typical chemical characteristics described by Drief and Nieto (2000) for detrital smectites in clastic sediments. Nevertheless, the presence of Mg-smectite should be related to the hydrothermal alteration produced by the laccolith.

The corrensite is characterized by a basal spacing of 29.9 Å (14.20 Å+15.70 Å) which expands to 31.55 Å after ethylene glycol treatment (14.20 Å+17.35 Å) (Figure 3). Heating to 550ºC causes a collapse to 24 Å. The different orders of the basal spacings define spacings with very small differences, which can always be interpreted as due to the low intensity or to the effect of the nearest peaks. Therefore, they can be considered as coherent with the smectite and chlorite layers forming an ordered interstratification of corrensite. At the lattice scale, corrensite zones of 14–10 Å fringe alternation can also be observed (Figure 8). Lattice-fringe images of regular chlorite-smectite interstratification commonly show lateral transition to smectite. In addition to the textural data, the AEM microanalyses are Si-Al poor and Mg-Fe rich, with an octahedral-cations total greater than that of a smectite plotting between saponite and chlorite in Figure 4. Their alternative normalization as chlorites (28 charges) produces a high Si content, a low sum of octahedral cations and a minor presence of interlayer cations, all the chemical characteristics described by Shau *et al.* (1990) as typical of corrensites. The structural formulae obtained from these analyses normalized to 25 charges (the sum of smectite and chlorite) (Table 4) produces a sum of octahedral cations near 4, is close to the ideal composition of an ordered interstratified trioctahedral chlorite-dioctahedral smectite. However, analyses of corrensite display Al deficits and an excess of Mg and Fe as compared with the theoretical

https://doi.org/10.1346/CCMN.2003.0510508 Published online by Cambridge University Press

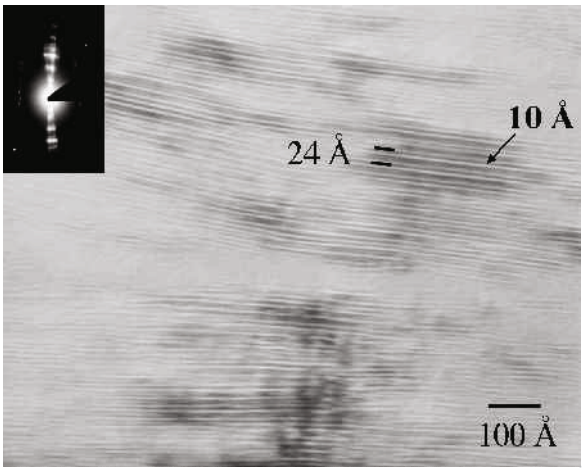

Figure 8. Lattice-fringe image of corrensite, with 24 Å periodicity = 10 Å (collapsed smectite) + 14 Å (chlorite), showing lateral transition to beidellitic smectite (10 Å periodicity) in coherence with AEM analyses (Table 3b) (sample Pr-15, Zone 2).

values of an ideal chlorite-dioctahedral smectite interstratification. The lattice image of Figure 8 reveals that smectite domains of ~100 Å thick exist inside the corrensite domains. This indicates that corrensite analyses could be contaminated by smectite. The XRD patterns prove the existence of both dioctahedral and trioctahedral smectites in the Zone 2 samples precluding any unambiguous identification of a dioctahedral-trioctahedral corrensite.

DISCUSSION

This sedimentological, mineralogical and petrological study contributes to an improved understanding of the sedimentation-magmatism interaction processes that have taken place during the evolution of the paleogeographic subdomain of the Median Subbetic since the early Jurassic.

Sedimentary context

In the pelagic marine environment of this subdomain during the Jurassic, there was a significant deposition of alternating limestones and marls at a depth of less than a few hundred meters (Molina and Vera, 1999, 2000). The Priego laccolith intruded the Toarcian-Aalenian sequence of the Zegrí Formation during the period of highest igneous activity (Aalenian-Bajocian) that affected the Median Subbetic. In the laccolith of the Sierra de San Pedro, Molina and Vera (2000) deduced that the intrusion took place just a few million years after the deposition of the host rocks. Considering the same sedimentation rate (~10–20 m/Ma) for the host rock of the Sierra de Priego laccolith, we can deduce that there may have been 50–100 m of host rock above the intrusion. The small age difference between the overlying sediments and the subvolcanic rocks suggest that the intrusion reached a near sea-floor area while the sediments were only partially consolidated. The presence of scar slumps in the Toarcian sediments developed by the doming produced by the intrusion also support this hypothesis.

This geological context favored the development of the mineralogical and textural changes that the intrusion of the subvolcanic body produced in the host rock during several stages of igneous-sedimentary interaction.

Contact metamorphism stage

The host-rock heating generated by the intrusion caused the crystallization of a paragenesis of calcic silicates during the contact metamorphism process. The upper temperature limit of the rocks closest to the contact with the intrusion may be constrained by the titanite disappearance curve (Moody *et al.*, 1983), which indicates temperatures below 500ºC.

The presence of andraditic rims in the garnets suggest the evolution of the metamorphism to higher conditions of oxygen fugacity, probably related to the presence of a fluid phase (Bird *et al.*, 1984; Jiménez-Millán and Velilla, 1994).

The thin zone of contact metamorphism (~9 m) is consistent with the small dimensions of the intrusive body. Bühmann (1992) reported that the effect of igneous intrusions on sedimentary rocks initially depends on the thickness of the intrusive body. Rowsell and De Swardt (1976) have even demonstrated the lack of metamorphism related to thin sills.

Hydrothermal alteration stage

The intense brecciation and the presence of clay minerals filling the vein network reveals the development and superimposition of a phyllosilicate association on the contact metamorphism paragenesis. The textural and chemical characteristics of the phyllosilicates suggest that they formed by the effect of hydrothermal

Table 4. Structural formulae for chlorite/smectite interstratifications normalized to $O_{10}(OH)_5$.

	Distance (m)	Si	^{IV}Al	^{VI}Al	Mg	Fe	Σoct	Na	K	Ca
Pr-15-8	18	3.54	0.46	1.22	2.10	0.59	3.92	0.00	0.00	0.21
Pr-15-7	18	3.34	0.66	0.99	2.50	0.58	4.07	0.00	0.00	0.25
Pr-15-6	18	3.59	0.41	1.22	2.21	0.48	3.91	0.00	0.00	0.18

AEM analyses. Total Fe assumed to be Fe^{2+}

https://doi.org/10.1346/CCMN.2003.0510508 Published online by Cambridge University Press

fluids circulating within the host rock. Despite the gradual cooling, the persistence of the calcic silicates in thermodynamic disequilibrium with the environment can be explained by their low dissolution rates.

A detailed study of phyllosilicates was considered as a key in the identification of hydrothermal processes. Clay mineral assemblages from other previously studied hydrothermal systems (Dudoignon *et al.*, 1997; Fulignati *et al.*, 1997; Hunter *et al.*, 1999) are zoned along the temperature gradient evolving from saponite to interstratified chlorite-smectite to chlorite. The same trend was observed in the thermal diagenesis of clay minerals within volcanogenic material (Vitali *et al.*, 1999) and the diagenesis of trioctahedral clays in sedimentary magmatic sequences (Sandler *et al.*, 2001). However, some studies have revealed that the proportion of chloritic layers is also influenced by the precursor minerals, the rock/fluid ratio, permeability conditions and variations in the composition of hydrothermal fluids (Shau and Peacor, 1992; Schiffman and Staudigel, 1995).

Saponite is the dominant phyllosilicate in the host-rock closest to the subvolcanic intrusion (Zone 1). Moreover, some dispersed chlorite crystals appear in this zone. Nonetheless, we have detected the presence of regular interstratified chlorite-smectite (corrensite) in a zone further from the contact (Zone 2), as well as saponite and beidellitic smectites. To account for this contrasting zoning, apparently opposed to that commonly developed in hydrothermal systems, we propose the following evolution model.

Prograde hydrothermal phase. The circulation of hot hydrothermal fluids by the vein network of the host rocks near the subvolcanic intrusion produced a zoning of clay minerals around the igneous body. Chlorite crystallized in the zone closest to the subvolcanic intrusion due to the circulation of highest-temperature fluids favored by the high fracture permeability of this zone. Corrensite was formed in the zone furthest away, which is less fractured and has a small column of partially consolidated sediments above the intrusion (50–100 m). This low overburden could have facilitated the circulation of lower-temperature fluids and may have allowed for the partial conservation of the original sedimentary dioctahedral smectites (beidellites), which are sometimes found together with quartz and calcite, incorporated into the veins as fragments of unreacted material. It is possible that this stage could have begun while Zone 1 was being affected by the contact metamorphism episode.

The presence of chlorite and corrensite was described in the highest-temperature zones of hydrothermal systems with a high content of magmatic fluids. Chlorite formation was determined as being ~300ºC (Dudoignon *et al.*, 1997), whereas the chlorite-smectite interstratification forms at temperatures of 200–270ºC (Stackes and O'Neil, 1982). In the studied rocks, this temperature can account for the K in the interlayers of the dioctahedral smectites which begin to change to illite-smectite at 70ºC. However, the XRD data do not prove illite interstratification in the Al-smectites from Zone 2.

Retrograde hydrothermal cooling phase. The existence of this stage is suggested by the massive presence of saponite in the zone closest to the intrusion, where intense fracturing once again facilitated the circulation of lower-temperature fluids that replaced the pre-existing hydrothermal association. This would account for the fact that only residual chlorite is found in Zone 1. Dudoignon *et al.* (1997) have described saponite as a retrograde hydrothermal phase in high-permeability zones and in the presence of heated fluids. Its genesis is favored by the influence of the infiltration of marine water, which causes a decrease in temperature down to values of 130–180ºC.

Finally, the small column of sediments above the intrusion (50–100 m) would have facilitated the participation of marine water in the interstitial fluids that reacted with the partially consolidated sediments. The retrograde hydrothermal process then culminated with the crystallization of Mg- and Na-rich saponite from a fluid mixture with a greater influence of marine water. The presence of scar slumps in the sediments overlying the laccolith suggest that the subvolcanic intrusion was almost contemporaneous with the host rocks.

Saponite is also present in Zone 2 samples, which indicates that retrograde hydrothermal fluids also affected the partially consolidated rocks furthest from the intrusion, thus revealing that the later hydrothermal stages do not correspond to the original zoning produced by contact metamorphism.

The processes of hydrothermal alteration have also affected the intrusive dolerites. Beidellite-type smectite was formed as the result of plagioclase alteration (Table 1). Drief *et al.* (2001) described the experimental genesis of Al-rich smectites from mafic subvolcanic rocks from the Sierra de San Pedro. They showed that interaction of the subvolcanic rock containing calcic plagioclase, pyroxene and olivine as major components with 1 M NaOH solution led to the formation of dioctahedral beidellite and Fe-rich montmorillonite after 1 and 3 days of reaction, respectively.

CONCLUSIONS

Combined sedimentological, mineralogical and petrological studies performed on the host rock and the igneous rock of a subvolcanic intrusion have allowed the detection of several effects of the sedimentary, magmatic, metamorphic and hydrothermal processes which occurred during the main phase of the Jurassic intracontinental rifting of the South Iberian continental margin. The subvolcanic intrusion took place at quite

https://doi.org/10.1346/CCMN.2003.0510508 Published online by Cambridge University Press

shallow depths below the ocean floor in partially consolidated sediments producing brecciation of the host rock. The doming related to the intrusion determined the pelagic sedimentation paleobathymetry and caused the formation of slumps. The zone closest to the subvolcanic intrusion initially developed a narrow contact metamorphism aureole consisting of calc-silicates, while the heating of fluids in the partially consolidated rocks furthest from the intrusion produced the beginning of the corrensite crystallization. The intense brecciation of rocks surrounding the intrusion favored the circulation of higher-temperature fluids, thus causing the formation of chlorite in this area. The thermal gradient evolved towards progressively cooler conditions producing a generalized retrograde event characterized by the saponite crystallization.

ACKNOWLEDGMENTS

We would like to thank N. Velilla (Univ. Granada) for his constructive comments, M.M. Abad (CIC, Univ. Granada) for her help with the HRTEM work and K. Livi (Johns Hopkins University) for his advice on the EMPA. We are also grateful to W.D. Huff and an anonymous reviewer for their helpful comments and suggestions. Christine Laurin and Marco Bettini are acknowledged for reviewing the English. The financial support was provided by Research Project BT2000-0582 (Spanish Ministry of Science and Technology) and the Research Groups RNM-179, RNM-200, RNM-208 and RNM-325 (Junta de Andalucía).

REFERENCES

Adamson, A.C. and Richards, H.G. (1990) Low temperature alteration of very young basalts from ODP Hole 648B: Serocki volcano Mid-Atlantic ridge. Pp. 106–109 in: *Proceedings of Ocean Drilling Program, Scientific Results* (R. Detrick, J. Honnorez, W.B. Bryan, R. Juteau *et al.*, editors). US Government Printing Officce, Washington, D.C.

Armstrong, J.T. (1989) *CITZAF: Combined ZAF and Phi-rho (Z) Electron beam correction Programs.* California Institute of Technology, Pasadena, California.

Bettison-Varga, L. and Mackinnon, I.D.R. (1997) The role of randomly mixed-layered chlorite/smectite in the transformation of smectite to chlorite. *Clays and Clay Minerals*, **45**, 506–516.

Bird, D.K., Schiffman, P., Elders, W.A., Williams, A.E. and McDowell, D.S. (1984) Calc-silicate mineralisation in active geothermal systems. *Economic Geology*, **79**, 671–695.

Bühmann, C. (1992) Smectite-to-illite conversion in a geothermally and lithologically complex Permian sedimentary sequence. *Clays and Clay Minerals*, **40**, 53–64.

Busnardo, R. and Chenevoy, M. (1962) Dolérites intrusives dans le Lias et le Dogger d'Andalousie; leurs différenciations pegmatitiques alcalines et auréoles de métamorphisme. *Bulletin de la Societé Geologique de France*, **7e serie, T-IV**, 461–470.

Clayton, T. and Pearce, R.B. (2000) Alteration mineralogy of Cretaceous basalt from ODP Site 1001, Leg 165 (Caribbean Sea). *Clay Minerals*, **35**, 719–733.

Decarreau, A., Grauby, O. and Petit, S. (1992) The actual distribution of octahedral cations in 2:1 clay minerals: Results from clay synthesis. *Applied Clay Science*, **7**, 147–167.

Drief, A. and Nieto, F. (2000) Chemical composition of smectites formed by clastic sediments. Implications of the smectite-illite transformation. *Clay Minerals*, **35**, 665–678.

Drief, A., Nieto, F. and Sánchez-Navas, A. (2001) Experimental clay-mineral formation from a subvolcanic rock by interaction with 1 M NaOH solution at room temperature. *Clays and Clay Minerals*, **49**, 92–106.

Dudoignon, P., Proust, D. and Gachon, A. (1997) Hydrothermal alteration associated with rift zones at Fangataufa Atoll (French-Polynesia). *Bulletin of Volcanology*. **58**, 583–596.

Einsele, G. (1986) Interaction between sediments and basalt injections in young Gulf of California-type Spreading Centers. *Geologische Rundschau*, **75**, 197–208.

Fulignati, P., Malfitano, G. and Sbrana A (1997) The Pantelleria-Caldera geothermal system – Data from the hydrothermal minerals. *Journal of Volcanology and Geothermal Research*. **75**, 251–270.

Grauby, O., Petit, S., Decarreau, A. and Baronnet, A. (1993) The beidellite-saponite series: An experimental approach. *European Journal of Mineralogy*, **5**, 623–635.

Honnorez, J. (1981) The aging of the oceanic crust at low temperature. Pp. 525–587 in: *The Sea* (E. Emiliani, editor). Wiley, New York.

Huertas, F.J., Cuadros, J., Huertas, F. and Linares, J. (2000) Experimental study of the hydrothermal formation of smectite in the beidellite-saponite series. *American Journal of Science*. **300**, 504–527.

Hunter, A.G., Kempton, P.D. and Greenwood, P. (1999) Low-temperature fluid-rock interaction – an isotopic and mineralogical perspective of upper crustal evolution, eastern flank of the Juan-de-Fuca ridge (Jdfr), ODP Leg-168. *Chemical Geology*, **155,** 3–28.

Jiménez Millán, J. and Velilla, N. (1994) Mineralogy and geochemistry of reduced manganese carbonate-silicate-rocks from the Aracena area (Iberian Massif, SW Spain). *Neues Jahrbuch für Mineralogie Abhandlungen*, **166**, 193–209.

Kelts, K. (1982) Petrology of hydrothermally metamorphosed sediments at Deep-Sea Drilling Site-477, Southern Guaymas basin rift, Gulf of California. *Initial Reports of the Deep Sea Drilling Project*, **64**, 1123–1136

Laverne, C. (1987) Les altérations des basaltes en domaine oceanique: minéralogie pétrologie et géochimie d'un système hydrothermal: le puits 504B, Pacifique oriental. PhD thesis, Université Aix-Marseille III, France, 315 pp.

Merriman, R.J., Bevins, R.E. and Ball, T.A. (1986) Petrological and geochemical variations within the Tal and Fan intrusion: a study of element mobility during low-grade metamorphism with implications for petrogenetic modelling. *Journal of Petrology*, **27**, 1409–1436.

Molina, J.M. and Vera, J.A. (1999) Sedimentación marina somera sobre edificios volcánicos submarinos (Jurásico medio-superior, Subbético Medio, Cordilleras Béticas). Pp. 91–106 in: *Libro Homenaje a José Ramírez del Pozo*. A.G.G.E.P., Madrid.

Molina, J.M. and Vera, J.A. (2000) Influencia del subvolcanismo en la sedimentación pelágica del Jurásico medio (Sierra de San Pedro, provincia de Jaén, Subbético medio). *Geogaceta*, **27**, 111–114.

Molina, J.M. and Vera, J.A. (2001) Cicatriz de *slump* en rocas pelágicas del Jurásico: su relación con el subvolcanismo (Priego de Córdoba, Zona Subbética). *Geogaceta*, **30**, 82–85.

Moody, J.B., Meyer, D. and Jenkins, J.E. (1983) Experimental characterization of the greenschist/amphibolite boundary in mafic systems. *American Journal of Science*, **283**, 48–92.

Nieto, F., Velilla, N., Peacor, D.R. and Ortega-Huertas, M. (1994) Regional retrograde alteration of sub-greenschist

facies chlorite to smectite. *Contributions to Mineralogy and Petrology*, **115**, 243–252.

Nieto, F., Ortega-Huertas, M., Peacor, D.R. and Aróstegui, J. (1996) Evolution of illite/smectite from early diagenesis through incipient metamorphism in sediments of the Basque-Cantabrian Basin. *Clays and Clay Minerals*, **44**, 304–323.

Ortega-Huertas, M., Palomo, I., Moresi, M. and Oddone, M. (1991) A mineralogical and geochemical approach to establishing a sedimentary model in a passive continental margin (Subbetic Zone, Betic Cordilleras, SE Spain). *Clay Minerals*, **26**, 389–407.

Peacor, D.R. (1992) Diagenesis and low-grade metamorphism of shales and slates. Pp. 113–140 in: *Minerals and Reactions at the Atomic Scales: Transmission Electron Microscopy* (P.R. Buseck, editor). Reviews in Mineralogy, **27**. Mineralogical Society of America, Washington, D.C.

Pichler, T., Ridley, W.I. and Nelson, E. (1999) Low-temperature alteration of dredged volcanics from the Southern Chile Ridge – additional information about early stages of sea-floor weathering. *Marine Geology*, **159**, 155–177.

Portugal, M., Morata, D., Puga, E., Demant, A. and Aguirre, L. (1995) Evolución geoquímica y temporal del magmatismo básico mesozoico en las Zonas Externas de las Cordilleras Béticas. *Estudios Geológicos*, **51**, 109–118.

Roberts, B., Morrison, C. and Hirons, S. (1990) Low grade metamorphism of the Manx Group, Isle of Man: a comparative study of white mica 'crystallinity' techniques. *Journal of the Geological Society of London*, **147**, 271–277.

Rowsell, D.M. and De Swardt, A.M.J. (1976) Diagenesis in Cape and Karoo sediments, South of Africa, and its bearing on their hydrocarbon potential. *Transactions of the Geological Society of South Africa*, **79**, 81–145.

Sandler, A., Nathan, Y., Eshet, Y. and Raab, M. (2001) Diagenesis of trioctahedral clays in a Miocene to Pleistocene sedimentary magmatic sequence from the Dead Sea Rift. *Clay Minerals*, **36**, 29–47.

Schiffman, P. and Fridleifsson G.O. (1991) The smectite-chlorite transition in drillhole NJ-15, Nesjavellir geothermal field, Iceland: XRD, BSE and electron microprobe investigations. *Journal of Metamorphic Geology*, **9**, 679–696.

Schiffman, P. and Staudigel, H. (1995) The smectite to chlorite transition in a fossil seamount hydrothermal system: The basament complex of La Palma, Canary Islands. *Journal of Metamorphic Geology*, **13**, 487–498.

Shau, Y.H. and Peacor, D.R. (1992) Phyllosilicates in hydrothermally altered basalts from DSDP hole 504B, leg 83-A TEM and AEM study. *Contributions to Mineralogy and Petrology*, **112**, 119–133.

Shau, Y.H., Peacor, D.R. and Essene, E.J. (1990) Corrensite and mixed-layer chlorite/corrensite in metabasalt from northern Taiwan: TEM/AEM, EMPA, XRD, and optical studies. *Contributions to Mineralogy and Petrology*, **105**, 123–142.

Stackes, D.S. and O'Neil, J.R. (1982) Mineralogy and stable isotope geochemistry of hydrothermally altered oceanic rocks. *Earth and Planetary Science Letters*, **57**, 285–304.

Vera, J.A., Molina, J.M., Montero, P. and Bea, F. (1997) Jurassic guyots on the southern Iberian Continental margin: a model of isolated carbonate platforms in volcanic submarine edifices. *Terra Nova*, **9**, 163–166.

Vitali, F., Blanc, G., Larque, P., Duplay, J. and Morvan, G. (1999) Thermal diagenesis of clay minerals within volcanogenic material from the Tonga Convergent Margin. *Marine Geology,* **157**, 105–125.

Yamada, H., Yoshioka, K., Tamura, K., Fujii, K. and Nakazawa, H. (1999) Compositional gap in dioctahedral-trioctahedral smectite system: Beidellite-saponite pseudo-binary join. *Clays and Clay Minerals*, **47**, 803–810.

(*Received 23 May 2002; revised 14 April 2003; Ms. 663 A.E. Warren D. Huff*)